Sound & Vibration 2026, 60(5), 4224.
doi: https://doi.org/10.59400/sv4224

Article

Weak fault feature extraction and system fault analysis under strong noise

Tiejun Cui[1,2], Zijian Cui[1], Shasha Li[1,2,*]

[1] School of Environmental and Chemical Engineering, Shenyang Ligong University, Shenyang 110159, China
[2] Liaoning Safety Engineering Industry School, Shenyang Ligong University, Shenyang 110159, China
*** Corresponding author:** Shasha Li, lsslntu@163.com

CITATION

Cui T, Cui Z, Li S. Weak fault feature extraction and system fault analysis under strong noise. Sound & Vibration. 2026; 60(5): 4224. https://doi.org/10.59400/sv4224

ARTICLE INFO

Received: 1 April 2026
Revised: 30 April 2026
Accepted: 6 May 2026
Available online: 23 July 2026

Abstract: To tackle the intractable problems including weak fault feature extraction and evolution uncertainty quantification for complex systems in strong noise environments, a novel method for weak fault diagnosis and evolution analysis is proposed. This method integrates the fuzzy structured element (FSE), cloud model (CM), and Space Fault Network (SFN). The method centers on adaptive wavelet denoising, fault feature cloudification, and SFN probability propagation. The fault signal under strong noise is reconstructed by optimizing the wavelet threshold with the FSE. The uncertainty encapsulation of the peak factor of fault features is realized based on the CM to establish the feature CM. The fault event topology is constructed relying on the SFN. The quantitative transfer of uncertainty in the fault evolution is achieved combined with cloud algebra. Verified by the inner ring pitting fault of axle box bearings, the results demonstrate that the proposed method can extract the fault characteristic frequency of 250.5 Hz. The derived fault probability CM (0.680, 0.059, 0.023) accurately quantifies the system risk level. This result is consistent with the actual fault evolution law in engineering practice. This method provides technical support for early fault warning and maintenance of complex industrial system. Furthermore, comparative experiments confirm its superiority over traditional methods in noise suppression and feature retention. Parameter analysis is also discussed to improve engineering generalization.

Keywords: strong noise; weak fault; feature extraction; uncertainty quantification; fault analysis

1. Introduction

With the development of modern industrial systems toward high speed and intelligence, core equipment such as high-speed trains and aero-engines has become increasingly complex. The operating status of their key components, such as bearings and gearboxes, directly determines the safety and reliability of the entire system. Such components are prone to weak faults such as micro-pitting and early spalling during long-term service due to multiple factors including load fluctuation and environmental erosion. In the early stage of faults, the signal amplitude is extremely low and masked by strong background noise such as wheel-rail impact and motor vibration. Traditional diagnosis methods are difficult to capture these signals. This leads to further fault evolution and causes serious safety accidents and economic losses.

At present, weak vibration fault feature diagnosis under strong noise has become a research hotspot in various fields.

Extracting weak fault features under strong noise background is the core difficulty in this field. Zou et al. [1] proposed an adaptive signal processing framework. It robustly extracts periodic weak features from vibration signals through intelligent spectrum optimization. This provides an effective tool for fault diagnosis under strong noise. Zhang et al. [2] adopted a variational filtering differential strategy combined with amplitude modulation. This enhances the fault feature extraction capability. Wang et al. [3] innovatively combined vibrational resonance in high-dimensional chaotic systems with variational mode decomposition. This realizes effective detection of weak faults. For early faults of rolling bearings, Liu et al. [4] improved the early fault feature extraction effect by fusing the GE and HOFMD methods. Shi et al. [5] proposed a two-stage chirp mode decomposition method guided by the generalized envelope nonlinear Gini index spectrogram. This solves the fault diagnosis problem of shield machine main bearings under complex working conditions. In terms of entropy index application, Liu et al. [6] proposed a new weak fault diagnosis method for bearings based on quadratic Manhattan entropy. This provides a new idea for the quantification of weak faults. In addition, Guo et al. [7] achieved accurate extraction of rolling bearing fault features through the improved IRBMO-CYCBD method.

The introduction of deep learning methods has opened a new path for fault diagnosis under strong noise. Aiming at strong noise interference, Zou et al. [8] proposed a multi-scale dilated convolutional neural network with dense connections. This effectively improves the robustness of bearing fault diagnosis. Chen et al. [9] designed a multi-scale adaptive quadratic convolutional network. This realizes reliable gearbox fault identification under severe noise environments. Wang et al. [10] combined parallel axial attention and residual networks. This improves the feature extraction capability of diagnosis models in noisy environments. In terms of lightweight models, Xu et al. [11] proposed the EPA-RepViT model. It is used for fault diagnosis of planetary gearboxes under strong noise. Li et al. [12] compared the effects of short-time Fourier transform, Mel spectrogram, and continuous wavelet transform in railway wheelset bearing fault diagnosis under strong noise based on the auditory perception mechanism. This verifies the effectiveness of the bionic method. Dong et al. [13] proposed a noise-robust method based on xLSTM. It is used for acoustic signal fault diagnosis of gas-insulated switchgear under strong noise interference. For multi-source sensor data, Li et al. [14] constructed the MSIF-Convformer end-to-end framework. This realizes effective fusion of multi-source information under strong noise conditions. Zhao et al. [15] realized the diagnosis of compound faults of rolling bearings through nonlinear convolutional sparse filtering combined with Gaussian fitting. In the application of deep reinforcement learning, Li et al. [16] improved the DQN framework. A dual residual horizontal feature pyramid was introduced to enhance the anti-noise ability of autonomous fault diagnosis.

Analyzing the fault evolution process from the system level is an important link to ensure industrial safety. Cui et al. [17] gave the partial differential analytical expression of the failure rate change of electrical components under multi-fault coupling. This provides a mathematical tool for system reliability analysis. This expands the application scenarios of fault analysis.

In summary, existing research has made remarkable progress in weak fault feature extraction under strong noise. The evolution from traditional signal processing to deep learning methods continuously improves the robustness of diagnosis. At the same time, system-level fault evolution analysis theories provide support for in-depth understanding of fault mechanisms. However, there are still some limitations. Most methods focus on single-link optimization and do not form a full-process system from signal processing to evolution evaluation. The uncertainty quantification of the System Fault Evolution Process (SFEP) is insufficient. It is difficult to accurately reflect the system risk state. The engineering applicability is limited. It is difficult to meet the needs of complex industrial scenarios. In addition, most studies lack sufficient parameter sensitivity analysis for key modules, resulting in poor model reproducibility. Meanwhile, the direct application of public fault datasets in strong noise-weak fault scenarios is limited, and the matching degree between simulation data and actual engineering noise characteristics needs to be further clarified, which restricts the practical popularization of the method.

To solve the above problems, a method for weak fault feature extraction and system fault analysis under strong noise is proposed. It integrates the FSE, CM, and SFN. An integrated framework of signal denoising-feature cloudification-evolution evaluation is constructed to solve the above problems. This method can not only realize early weak fault identification under strong noise environments but also quantify fault evolution risk and uncertainty. It provides theoretical support and engineering solutions for the maintenance and support of complex industrial systems.

The primary contributions of this study (centered on the integrated framework of FSE, CM, and SFN) are as follows.

- It reveals the noise suppression mechanism of FSE wavelet threshold denoising and the uncertainty encapsulation law of the CM. It clarifies that weak fault feature extraction under strong noise depends on adaptive denoising to retain impact components. It expounds the quantitative transmission rule of fault uncertainty driven by the synergy of feature cloudification and SFN probability propagation.
- It constructs a weak fault feature extraction and system fault evolution quantification model embedded in the integrated framework. It realizes adaptive denoising of strong noise vibration signals via the FSE. It completes uncertainty characterization of fault feature peak factor through the CM. It decomposes the fault evolution process into event topology and logic transmission by the SFN. It proposes a fault risk quantification criterion based on cloud digital characteristics.
- It verifies the integrated framework's effectiveness with axle box bearing inner ring pitting fault as an example. It extracts 250.5 Hz fault characteristic frequency under -5 dB strong noise. It obtains the fault probability CM Ex to quantify system risk. It clarifies the application value of fuzzy denoising, feature cloudification, and SFN evolution in early fault warning. It provides a technical scheme for weak fault analysis of complex industrial systems. Meanwhile, parameter sensitivity analysis and public dataset applicability discussion are supplemented to optimize the model parameter configuration and data application scope, and the stability and engineering adaptability of the method are further improved.

It should be noted that the theoretical frameworks employed in this paper have been separately applied in our previous research for signal processing, uncertainty characterization, and system fault evolution analysis. The incremental contribution of this work lies in the first organic integration of these three theories to construct a unified model for mechanical weak fault diagnosis and evolution risk assessment under strong noise environments. Specifically, this study extends the application of FSE in wavelet threshold denoising to adapt to bearing impulse signals, utilizes CM to quantify the uncertainty of envelope spectrum feature factors after denoising, and finally implements system-level fault state evolution assessment based on probability clouds via SFN. Thus, the core innovation of this paper is the integrated methodological innovation and its validation in a new application scenario (mechanical faults under strong noise), rather than the proposal of individual foundational theories.

This study is organized as follows. Section 2 introduces the problem statement. Section 3 details the proposed mathematical model. Section 4 presents the case analysis and discussions. Section 5 provides the conclusions.

2. Problem statement

In complex industrial systems such as high-speed train axle box bearings, aero-engine gearboxes, and marine motor rotors, weak faults such as early micro-pitting and slight spalling are prone to occur. The vibration fault signals generated by these faults have extremely low amplitudes. They are submerged by strong background noise such as wheel-rail impact, mechanical coupling, and environmental interference. For example, axle box bearings are affected by superposition of wheel-rail vibration and motor noise during operation. The signal-to-noise ratio (SNR) of the inner ring early pitting fault vibration characteristic can be as low as −5 dB. Traditional methods are difficult to effectively identify such faults. This leads to faults such as axle box overheating and seizure, threatening equipment safety.

Its essence is the robust extraction of weak fault features under strong noise interference. It also involves the quantification and transmission of multi-factor uncertainty in fault evolution. Strong noise masks fault impact features. Traditional methods are difficult to retain weak fault information while suppressing noise. Fault occurrence and evolution are multi-event logically correlated processes. The randomness and fuzziness of feature extraction and fault propagation cannot be characterized by deterministic analysis. This leads to large deviations between fault probability evaluation and actual conditions. Theoretically, this study can improve the uncertainty analysis of fault feature extraction under strong noise environments. It provides a mathematical model for the quantification of mechanical fault diagnosis. In engineering, it can realize the identification and fault evolution analysis of early weak faults of key components in complex industrial systems. It provides technical support for equipment maintenance and early fault warning in fields such as high-speed trains, aerospace, and marine engineering.

The FSE is a theory in the field of fuzzy systems and mathematics [18]. It characterizes the distribution characteristics of fuzzy sets through regular FSEs on the real number domain, such as triangular and normal structural elements. It transforms the operation of fuzzy-valued functions into the composite operation of structural elements and real-valued functions. This realizes the quantitative description of fuzzy information. It is widely used in fuzzy signal processing, uncertainty decision-making, fault diagnosis and other fields. In this paper, it is used to characterize the discrete distribution characteristics of noise wavelet coefficients and construct an adaptive wavelet threshold function.

The CM was proposed by Li et al. [19]. It is a mathematical model that realizes the uncertainty conversion between qualitative concepts and quantitative values. It is widely used in reliability analysis, data mining, fault feature characterization and other fields. In this paper, it is used for the cloudification characterization of fault feature peak factors calculated multiple times. It encapsulates the uncertainty in the feature extraction process and provides a feature factor model containing random and fuzzy information.

The Hilbert envelope demodulation theory is developed based on the Hilbert transform [20]. The analytic signal is constructed by performing Hilbert transform on the vibration signal. The envelope signal of the original signal is obtained through the modulus of the analytic signal. The envelope spectrum is obtained by performing Fourier transform on the envelope signal. This extracts amplitude modulation features. This theory is a classical method for extracting fault characteristic frequencies in mechanical fault diagnosis. It is widely used in fault diagnosis of rolling bearings, gearboxes and other components. In this paper, it is used for processing denoised vibration signals to extract fault characteristic frequency components.

The SFN was proposed by scholars Cui and Li [21]. It is a network model describing the SFEP. Various events of the SFEP are defined as nodes. The causal and logical relationships between events are defined as edges. Quantitative analysis of the SFEP is realized through network topology and logical operations. It is used in fault evolution analysis and risk assessment of complex systems. In this paper, it serves as the core framework for fault evolution analysis. The cloudified fault feature factors are integrated into the network as influencing factors. The transmission and quantification of fault uncertainty are realized combined with cloud algebra. Finally, the CM of the system fault occurrence probability is obtained.

Wavelet transform is a classical time-frequency localization analysis method [22]. The original signal is decomposed into multi-scales through scaling and shifting of wavelet basis functions. It has the advantages of both time-domain and frequency-domain analysis. It is applied in signal denoising, feature extraction, data compression and other fields. In this paper, it is used as a signal denoising method. The vibration signal is decomposed into multi-scale coefficients through discrete wavelet transform (DWT). Threshold processing and signal reconstruction are performed combined with the FSE.

3. Establishment of mathematical model

3.1. Problems in method research

Traditional fault diagnosis methods, such as empirical mode decomposition and wavelet packet decomposition, have problems such as poor feature extraction effect, information redundancy, and easy misdiagnosis under strong noise environments [23]. At the same time, fault occurrence is not an isolated event. It is an evolution process driven by multiple factors and logically correlated by multiple events. Therefore, the core problem to be solved by the method is to robustly extract weak feature factors that can characterize the fault state from strong noise signals. The uncertainty characteristics are taken as influencing factors and input into the SFN describing the SFEP. Quantitative evolution analysis and probability evaluation are then carried out.

3.2. Basic idea of the method

An integrated model framework of signal denoising-feature cloudification-evolution evaluation is constructed. The CM and FSE are integrated into the signal processing and feature extraction process. This enhances the robustness to strong noise and uncertainty. The extracted uncertainty features are taken as influencing factors using factor space. They are deeply integrated with the SFN to realize probabilistic and uncertainty quantification of the SFEP.

Anti-noise preprocessing: The FSE-based wavelet threshold denoising method is adopted for strong noise vibration signals. The FSE characterizes the discrete distribution characteristics of noise. It realizes adaptive processing of wavelet coefficients. It maximizes the retention of weak fault impact components while suppressing noise.

Feature factor extraction and cloudification: Hilbert envelope demodulation is performed on the denoised signal to obtain the envelope spectrum. The fault feature peak factor is defined. It quantifies the prominence degree of energized fault frequency components relative to background noise. Due to noise interference, the single calculated factor value has randomness and fuzziness. Therefore, the CM is used to characterize the factor values obtained from multiple calculations. A cloudified feature factor described by expectation Ex, entropy (0.680,0.059,0.023)En, and hyper-entropy He is obtained.

SFN evolution analysis of cloudified features: The cloudified feature factors are taken as influencing factors in the SFN. A cloudified feature function is constructed. It takes the CM as input and outputs the CM representing the event occurrence probability. Through the network topology of the SFN and logical relationships between events, namely AND, OR, and TRANSFER, probability propagation calculation is performed using cloud algebra. The CM of the final system fault occurrence probability is obtained. The fault probability expectation estimation and the uncertainty of the evaluation process are obtained.

3.3. Brief steps of the method

1) Signal acquisition and preprocessing: Collect system vibration signals under strong noise. Perform necessary filtering and standardization.
2) FSE-based wavelet denoising: Use the FSE to construct an adaptive wavelet threshold function. Denoise the signal and highlight fault impact features.
3) Envelope spectrum analysis and feature factor calculation: Perform Hilbert envelope demodulation on the denoised signal to calculate the envelope spectrum. Extract the fault feature peak factor for specific fault types.

4) CM characterization of feature factors: Perform inverse cloud transformation on the feature factor values calculated from consecutive multiple data segments. Generate the CM $C(Ex, En, He)$ characterizing the feature factor.
5) Construct SFN model of the SFEP: Establish the SFN describing the SFEP according to the system structure and fault mechanism. Clarify the edge events, process events, final events, and their logical relationships and transmission probabilities.
6) Define cloudified feature function: Establish a mathematical function mapping cloudified feature factors to the CM of event occurrence probability.
7) SFN cloudified probability calculation: Take cloudified feature factors as influencing factors and substitute them into the cloudified feature function. Calculate the CM of occurrence probability of each event. According to the logical relationship of the SFN, use cloud algebra for probability synthesis. Calculate the CM of the final system fault occurrence probability $P_T\left(Ex_T, En_T, He_T\right)$.
8) Result analysis and decision-making: Judge the system risk level according to the expected value Ex_T of the final fault probability CM. Evaluate the confidence and uncertainty of the risk conclusion combined with entropy En_T and hyper-entropy He_T.

3.4. Detailed steps and mathematical model

3.4.1. FSE wavelet threshold denoising

Extract the weak fault impact signal $s(t)$ from the strong noise $n(t)$. The observed signal is $x(t) = s(t) + n(t)$. The main steps are given below.

1) Wavelet decomposition: Select the wavelet basis function $\psi(t)$ to perform L-layer DWT on the signal $x(t)$. Let $\phi(t)$ be the scaling function corresponding to $\psi(t)$. The approximation coefficient $a_{j,k}$ and detail coefficient $d_{j,k}$ of the signal $x(t)$ at scale j are shown in Equations (1) and (2), respectively.

$$a_{j,k} =< x(t), \phi_{j,k}(t) >= \int_{-\infty}^{\infty} x(t) \cdot 2^{-j/2}\phi\left(2^{-j}t - k\right) dt, \tag{1}$$

$$d_{j,k} =< x(t), \psi_{j,k}(t) >= \int_{-\infty}^{\infty} x(t) \cdot 2^{-j/2}\psi\left(2^{-j}t - k\right) dt. \tag{2}$$

Where: $j = 1, 2, \ldots, L$ is the decomposition scale (layer number), k is the translation parameter. $\phi_{j,k}(t)$ and $\psi_{j,k}(t)$ are the scaling and shifting forms of the scaling function and wavelet function respectively. In actual discrete sampling signals, the above transform is realized through iterative convolution and downsampling of filter banks, namely low-pass filter h and high-pass filter g.
2) Construct FSE to characterize noise: The FSE E is introduced to characterize the discrete distribution characteristics of noise wavelet coefficients [24]. Let E be a regular FSE on the real number field $\mathbb{R}$ with membership function $E(x)$, usually a triangular or normal structural element. The fluctuation characteristics of $d_{j,k}$ affected by noise are described by a fuzzy-valued function linearly generated by

E. The fuzzy threshold function is defined as shown in Equation (3).

$$T_E\left(d_{j,k}\right) = \text{sign}\left(d_{j,k}\right) \cdot \max\left(\left|d_{j,k}\right| - \lambda_j \cdot \mu_E\left(\left|d_{j,k}\right|\right), 0\right). \tag{3}$$

Where: λ_j is the global threshold of layer j, usually taken as $\lambda_j = \sigma_j\sqrt{2\ln N}$. σ_j is the median absolute deviation (MAD) estimation of the detail coefficients of layer j, $\sigma_j = \frac{\text{MAD}_j}{0.6745}$, $\text{MAD}_j = \text{median}\{|d_{j,k} - \text{median}\{d_{j,k}\}|\}(k = 1, 2, \ldots, N)$. N is the signal length. $\mu_E\left(\left|d_{j,k}\right|\right)$ is the membership function based on the FSE E. It is used to dynamically adjust the threshold shrinkage intensity according to the absolute coefficient value $|d_{j,k}|$, as shown in Equation (4).

$$\mu_E\left(\left|d_{j,k}\right|\right) = \frac{E\left(\frac{|d_{j,k}| - m_j}{s_j}\right) + 1}{2}. \tag{4}$$

Where: m_j and s_j are statistics of the absolute values of the detail coefficients of layer j, such as median and interquartile range. They are used to map the coefficient values to the definition domain of the FSE E, usually [−1,1]. The value range of $\mu_E(\cdot)$ is [0.5,1]. When $|d_{j,k}|$ is small, μ_E is close to 1. It indicates that the coefficient is likely to be noise and strong threshold shrinkage is performed. When $|d_{j,k}|$ is large, μ_E is close to 0.5. It indicates that the coefficient may be a fault impact and weak shrinkage is performed to better retain fault features.

3) Threshold processing and coefficient reconstruction: Apply the fuzzy threshold function $T_E(\cdot)$ to the detail coefficients $|d_{j,k}|$ of each layer. The processed detail coefficients $\widehat{d}_{j,k} = T_E\left(d_{j,k}\right)$ are obtained. The approximation coefficients $a_{L,k}$ are usually kept unchanged.
4) Wavelet reconstruction: Use the processed coefficients $\{\widehat{d}_{j,k}\}$ and $\{a_{L,k}\}$ to perform inverse discrete wavelet transform (IDWT). Reconstruct to obtain the denoised signal $\widehat{x}(t)$, as shown in Equation (5). In the actual discrete algorithm, reconstruction is realized through upsampling and convolution of the corresponding reconstruction filter banks $\widetilde{h}$ and $\widetilde{g}$.

$$\widehat{x}(t) = \sum\nolimits_k a_{L,k}\phi_{L,k}(t) + \sum\nolimits_{j=1}^{L}\sum\nolimits_k \widehat{d}_{j,k}\psi_{j,k}(t). \tag{5}$$

Compared with traditional methods, the FSE threshold method realizes adaptive threshold shrinkage through $\mu_E(\cdot)$. It can judge the probability of coefficients belonging to noise or signal according to the coefficient value size. Thus, it suppresses noise while better retaining larger coefficients representing fault impacts and improves denoising ability [24].

3.4.2. Fault feature peak factor extraction and cloudification

A quantifiable fault feature index is extracted from the denoised signal $\widehat{x}(t)$ and its uncertainty is processed.

1) Envelope spectrum analysis: Perform Hilbert transform on $\widehat{x}(t)$ to obtain the envelope spectrum. The Hilbert transform $\mathcal{H}[\cdot]$ is shown in Equation (6). The analytic signal is constructed as shown in Equation (7). The signal envelope $e(t)$

is the modulus of the analytic signal, as shown in Equation (8). Discrete Fourier transform (DFT) is performed on the envelope signal $e(t)$ to obtain the envelope spectrum, as shown in Equation (9).

$$\widehat{x}_H(t) = \mathcal{H}[\widehat{x}(t)] = \frac{1}{\pi}\text{P.V.}\int_{-\infty}^{\infty} \frac{\widehat{x}(\tau)}{t-\tau} d\tau = \frac{1}{\pi} \underset{\varepsilon \to 0^+}{lim} \left[\int_{-\infty}^{t-\varepsilon} \frac{\widehat{x}(\tau)}{t-\tau} d\tau + \int_{t+\varepsilon}^{\infty} \frac{\widehat{x}(\tau)}{t-\tau} d\tau\right]. \tag{6}$$

Where: P.V. represents the Cauchy principal value.

$$z(t) = \widehat{x}(t) + j \cdot \widehat{x}_H(t), \tag{7}$$

$$e(t) = |z(t)| = \sqrt{\widehat{x}^2(t) + \widehat{x}_H^2(t)}, \tag{8}$$

$$S(f) = \left|\sum_{n=0}^{N-1} e[n] \cdot e^{-j2\pi fn/N}\right|, f = 0, \frac{f_s}{N}, ..., \frac{f_s(N-1)}{N}. \tag{9}$$

Where: $e[n]$ is the discrete sampling of $e(t)$, N is the number of sampling points, f_s is the sampling frequency.

2) Calculate fault feature peak factor: The peak factor for a specific fault type q is defined as shown in Equation (10).

$$F_q = \frac{\max\limits_{w \in \{1,2,...,W\}} S\left(f_q^{(w)}\right)}{\frac{1}{N_f}\sum_{f=1}^{N_f} S(f)}. \tag{10}$$

Where: $f_q^{(w)}$ is the w-th multiple characteristic frequency of fault type q, $w = 1, 2, \ldots, W$. W is the number of considered multiples, usually 3–5. $S(f)$ is the amplitude of the envelope spectrum at frequency f. N_f is the number of frequency points of the envelope spectrum, usually $N/2$. The denominator is the average amplitude of the envelope spectrum, representing the overall level of background noise and harmonics. F_q is the multiple of the maximum amplitude at the fault characteristic frequency and its multiples relative to the average background. The larger the value, the more obvious the fault features.

The denominator in Equation (10) for employs the global average amplitude of the entire envelope spectrum as the background noise estimate. This definition is effective in most cases. However, in practical engineering applications, if the signal contains strong interfering frequency components unrelated to the fault (e.g., gear meshing frequency, motor harmonics), these components can significantly inflate the denominator's value, thereby artificially suppressing the value and potentially masking the genuine fault. This represents a potential limitation of the current indicator definition. To enhance the robustness of the indicator against strong interferences, a feasible improvement is to adopt a local background noise estimate, for instance, calculating the neighborhood average amplitude around the fundamental fault characteristic frequency while excluding narrow bands near the fault frequency and its multiples, denoted as the local background estimate Future work will explore the construction of more robust feature indicators of this kind.

3) CM characterization: Due to residual noise and working condition fluctuations, the single calculated F_q is unstable. M consecutive signal segments are intercepted

and calculated respectively to obtain the sequence $\left\{F_q^{(m)}\right\}$, $m = 1, \ldots, M$. The inverse cloud transformation is performed on this sequence to generate the CM $C_q\left(Ex_q, En_q, He_q\right)$. Ex is the sample mean of the sequence, representing the central estimated value of the feature factor, as shown in Equation (11). En_q is the dispersion degree and fuzziness of the feature factor, namely the fluctuation range, as shown in Equation (12). He_q is the uncertainty of entropy En_q, namely the stability degree of the fluctuation range itself, as shown in Equation (13).

$$Ex_q = \frac{1}{M} \sum\nolimits_{m=1}^{M} F_q^{(m)}, \tag{11}$$

$$En_q = \sqrt{\frac{\pi}{2}} \times \frac{1}{M} \sum\nolimits_{m=1}^{M} \left| F_q^{(m)} - Ex_q \right|, \tag{12}$$

$$He_q = \sqrt{\frac{1}{M-1} \sum\nolimits_{m=1}^{M} \left(F_q^{(m)} - Ex_q \right)^2 - \left(En_q\right)^2}. \tag{13}$$

The CM C_q extends the feature factor from a definite value to a mathematical object with probability distribution characteristics. It retains its randomness and fuzziness information.

3.4.3. Cloudified feature factor input to SFN

Integrate uncertainty features into system fault evolution analysis.

1) Construct SFN model: Establish the SFN according to the system fault mechanism, $G = (V, E, L)$ [21]. Where V is the set of event nodes, including edge events V_e, process events V_p, and final events V_f. $E \subseteq V \times V$ represents the set of directed edges for causal evolution relationships. *L: E* → {AND, OR TRANSFER} is the mapping of logical relationships on edges.
2) Define cloudified feature function: Let event $e_i \in V_e$ be affected by influencing factor f_k, namely cloudified feature factor C_k. The cloudified feature function $\Phi_{ik}^{\text{cloud}} : C_k \to P_{ik}^{\text{cloud}}$ is defined. It maps the CM $C_k\left(Ex_k, En_k, He_k\right)$ to the CM $P_{ik}^{\text{cloud}}\left(Ex_{ik}^{p}, En_{ik}^{p}, He_{ik}^{p}\right)$ of the occurrence probability of event e_i under the action of factor f_k. It is defined based on the normal cloud and probability mapping as shown in Equation (14).

$$Ex_{ik}^{p} = \Psi\left(\frac{Ex_k - \theta_{ik}}{\eta \cdot En_k}\right). \tag{14}$$

Where: $\Psi(\cdot)$ is the cumulative distribution function of the standard normal distribution, namely $\Psi(z) = \frac{1}{\sqrt{2\pi}} \int_{-\infty}^{z} e^{-t^2/2} dt$; θ_{ik} is the threshold of event e_i affected by factor f_k. When the expected value Ex_k of the feature factor exceeds this threshold, the event occurrence probability increases significantly. η is the adjustment coefficient, usually $\eta > 0$, used to control the rate of probability change with the feature factor. En_k in the denominator means that the greater the fuzziness of the feature factor itself, the gentler the probability change leading to event occurrence.

The entropy En_{ik}^{P} and hyper-entropy He_{ik}^{P} of the probability cloud are determined through the uncertainty propagation function. They reflect the transmission of input cloud uncertainty to the output probability cloud. The simplified method is to set $En_{ik}^{p} \propto He_k$, $He_{ik}^{p} \propto std\left(He_k\right)$, or determine through Monte Carlo simulation.

The cloudified feature function $P_f^{cloud}(x)$ defined in Equation (14) serves as the critical bridge mapping the feature cloud (Ex, En, He) to the fault probability cloud. Its design is based on the following rationale. First, the cumulative normal distribution function $\Phi(\cdot)$ is chosen as the S-shaped mapping function because the normal distribution has a theoretical foundation in uncertainty propagation and probability transformation rooted in the central limit theorem. Moreover, in the cloud model, the normal distribution defined by expectation Ex and entropy En is the fundamental form for describing qualitative concepts [19]. Second, entropyEn, rather than hyper-entropy He, is used in the denominator to control the slope of the probability curve. This is because En characterizes the dispersion degree of feature values around the expectation Ex (i.e., first-order uncertainty), which directly determines the rate of change in the likelihood that a feature value falls into the 'fault' state interval. Hyper-entropy He, representing the uncertainty of entropy En (second-order uncertainty), primarily affects the thickness of cloud drop distribution [19]. Using He in the denominator would overly complicate the probability mapping and obscure its physical meaning. Therefore, the design based on En ensures that the probability mapping is primarily driven by the first-order uncertainty of the feature, which aligns with the idea of utilizing En to construct membership or probability functions in other cloud-model-based decision-making methods (e.g., constructing basic probability assignment functions using En). This design results in the maximum slope of the probability curve at Ex, reflecting that the probability of belonging to the fault state changes most sensitively when the feature value is close to its expectation.

3) Calculate the CM of edge event occurrence probability: For edge event e_i, its occurrence probability CM $P^{\text{cloud}}\left(e_i\right)$ is jointly determined by all cloudified feature factors affecting it. It is usually assumed that factors are independent. OR logic synthesis is adopted, namely any sufficient factor can lead to event occurrence, as shown in Equation (15).

$$P^{\text{cloud}}\left(e_i\right) = 1 - \prod_{k=1}^{K_i} \left(1 - P_{ik}^{\text{cloud}}\right). \tag{15}$$

The multiplication $\prod$ and subtraction operations in Equation (15) need to be performed under the cloud algebra framework. Cloud algebra operations use approximate computations on the digital characteristics(Ex, En, He) of the cloud, or more precisely through cloud drop operations. Cloud drop operations generate a large number of cloud drops from each input CM P_{ik}^{cloud} respectively. Arithmetic operations of Equation (15) are performed on these sample points to obtain the output cloud drop set. Then forward cloud transformation is performed on the set to obtain the digital characteristics of the output cloud $P^{\text{cloud}}(e_i)$.

4) SFN probability propagation and final event probability calculation: Probability propagation is performed from edge events to final events according to the network topology and logical relationship of the SFN. Let the transmission probability of

edge $e_{cr} \to e_j$ be $tp_{cr \to j}$, a definite value or a CM. AND logic: if $L(e_{cr} \to e_j) =$ AND and e_j has R cause events, calculate according to Equation (16). OR logic: if $L(e_{cr} \to e_j) =$ OR, calculate according to Equation (17). Transfer relationship: regarded as AND logic with $R = 1$. Finally, the CM of the system fault event $e_F \in V_f$ is obtained, as shown in Equation (18).

$$P^{\text{cloud}}(e_j) = \prod_{r=1}^{R} \left[P^{\text{cloud}}(e_{cr}) \odot tp_{cr \to j} \right], \tag{16}$$

$$P^{\text{cloud}}(e_j) = 1 - \prod_{r=1}^{R} \left[1 - P^{\text{cloud}}(e_{cr}) \odot tp_{cr \to j} \right], \tag{17}$$

$$P_T^{\text{cloud}} = P^{\text{cloud}}(e_F) = (Ex_T, En_T, He_T). \tag{18}$$

The above method constructs a system fault analysis framework capable of handling strong noise and uncertainty by integrating FSE wavelet denoising, CM feature characterization, and SFN evolution analysis. It can not only robustly extract weak fault features but also quantify and transmit the uncertainty of the entire process of feature extraction and evolution analysis. Finally, it outputs a CM result containing probability expectation and its uncertainty. The overall flow chart of the method is shown in **Figure 1**.

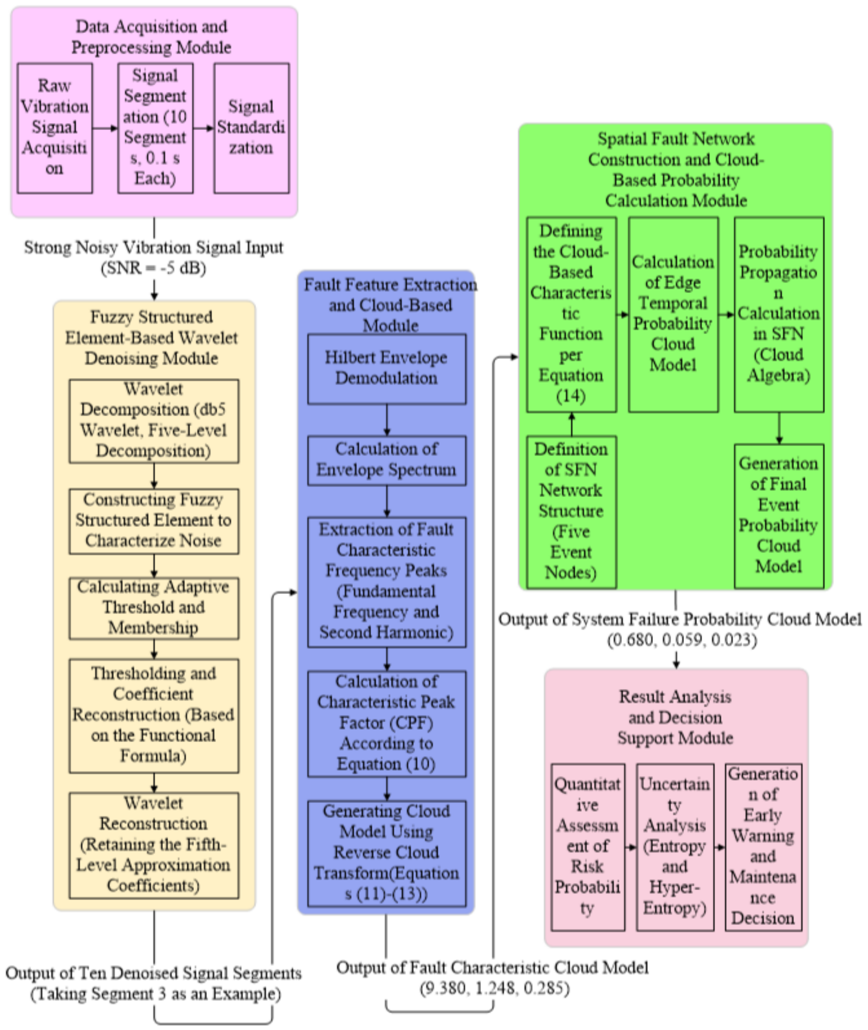

Figure 1. Flowchart of the proposed method.

4. Case analysis

This study takes the axle box rolling bearing as the object. Bearings are key components of train running gear. Their early faults, such as micro-pitting and early spalling of inner rings, outer rings or rolling elements, produce extremely weak vibration signals. These signals are submerged in strong wheel-rail impact noise, motor vibration noise and environmental noise of trains [23]. Accurate extraction of early fault features and evaluation of their safety for train operation have important engineering significance.

4.1. Research environment and raw data

This study considers wheel-rail excitation, motor torque fluctuation, bearing nonlinear contact force and fault impact for data simulation [23]. Fault setting: an early pitting fault is set on the inner ring of the bearing. Noise environment: Gaussian white noise is superimposed on the vibration signal. The SNR is set to −5 dB to simulate a strong noise environment. Sampling parameters: sampling frequency $f_s = 25,600$ Hz, simulation duration $T = 2$ s, a total of $N = 51,200$ data points are obtained. The vibration signal $x(t)$ is the vertical acceleration signal. Bearing parameters: number of rolling elements $Z = 17$, pitch diameter $D_m = 190$ mm, rolling element diameter $d = 34$ mm, contact angle $\alpha = 0°$. According to the bearing geometric parameters and train running speed, set to $n = 1,500$ rpm, the inner ring fault characteristic frequency (Ball Pass Frequency Inner, BPFI) is calculated as $f_{BPFI} = \frac{Z}{2}\left(1 + \frac{d}{D_m}\cos\alpha\right)\frac{n}{60} \approx 250.5$ Hz.

The original vibration acceleration signal $x[n](n = 1, ..., 51, 200)$ with strong noise is obtained from the data. 10 consecutive representative 0.1 s data segments, 2,560 points per segment, are intercepted to calculate their key features. The raw signal segments and preliminary statistics are shown in **Table 1**.

Table 1. Segment data of the original vibration signal.

Data segment number	Time range (s)	Signal segment peak value (m/s^2)	Root mean square (RMS)(m/s^2)	Kurtosis
1	0.0–0.1	0.11	0.03	3.29
2	0.1–0.2	0.12	0.03	3.23
3	0.2–0.3	0.10	0.03	3.23
4	0.3–0.4	0.11	0.03	3.55
5	0.4–0.5	0.13	0.03	3.39
6	0.5–0.6	0.10	0.03	3.27
7	0.6–0.7	0.11	0.03	3.46
8	0.7–0.8	0.09	0.03	3.02
9	0.8–0.9	0.12	0.03	3.30
10	0.9–1.0	0.11	0.03	3.14

It can be seen from the kurtosis value close to 3, the kurtosis of Gaussian distribution, that the signal is dominated by strong noise and the fault impact features are not obvious.

4.2. Case analysis and calculation results

Step 1: FSE wavelet threshold denoising

Wavelet decomposition: Select the $db10$ wavelet as the basis function $\psi(t)$.

Perform 5-layer ($L = 5$) discrete wavelet decomposition on each data segment $x_m[n]$. Obtain the approximation coefficients $a_{5,k}^{(m)}$ and detail coefficients $d_{j,k}^{(m)}$ of each layer according to Equations (1) and (2).

Construct FSE and threshold function: Adopt the triangular FSE E with membership function $E(x) = \max(0, 1 - |x|)$ and definition domain $[-1, 1]$. Calculate the adaptive membership degree $\mu_E(|d_{j,k}|)$ of each layer coefficient according to Equation (4). Where m_j is taken as the median of the absolute values of the detail coefficients of layer j, s_j is taken as its interquartile range. The global threshold λ_j is calculated according to the universal threshold $\lambda_j = \sigma_j\sqrt{2\ln(2,560)}$. σ_j is the MAD estimation of the detail coefficients of layer j.

Threshold processing and reconstruction: Process the detail coefficients of each layer according to the $T_E(\cdot)$ function in Equation (3). Keep the 5th-layer approximation coefficients unchanged. Perform wavelet reconstruction according to Equation (5) to obtain 10 denoised signal segments $\widehat{x}_m[n]$. The denoising effect comparison is shown in **Table 2**, taking data segment 3 as an example.

Table 2. Comparison of signal characteristics before and after wavelet denoising.

Indicator/index	Original signal $x_3[n]$	Denoised signal via fuzzy structuring element thresholding $\widehat{x}_3[n]$
Peak (m/s^2)	0.10	0.07
RMS (m/s^2)	0.03	0.01
Kurtosis	3.23	4.66
SNR Improvement (dB)	−5	4.9

The FSE method in **Table 2** further reduces the RMS, noise level, while retaining a higher peak value and obtaining a larger kurtosis value. This indicates that it better retains fault impact components and the SNR improvement is more significant. The time-domain comparison between the original vibration signal and the FSE wavelet denoised signal is shown in **Figure 2**.

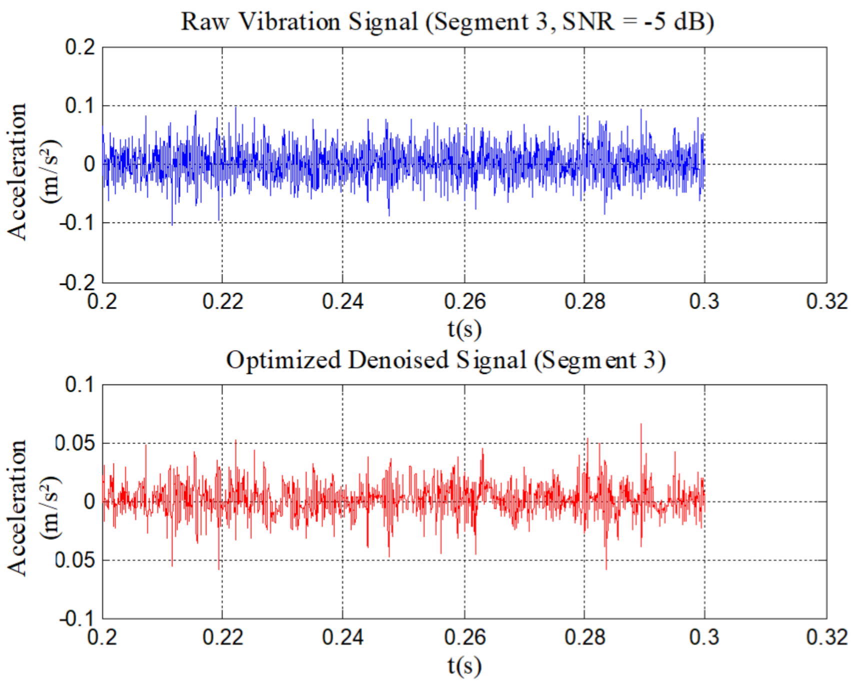

Figure 2. Comparison between the original vibration signal and the denoised signal.

Figure 2 shows the time-domain comparison of the vibration signal of the 3rd segment with a duration of 0.1 s. The upper part is the original signal with SNR $= -5$ dB. The waveform presents irregular strong noise characteristics. Fault impacts are submerged and there are no obvious periodic impact signals. The lower part is the signal after FSE wavelet threshold denoising. Noise is greatly suppressed. Periodic impact pulses matching the inner ring fault characteristic frequency can be clearly identified. The impact amplitude consistency is good. The comparison between the two figures reflects that the proposed denoising method can effectively suppress Gaussian white noise while retaining fault features in strong noise environments.

Step 2: Fault feature peak factor extraction and cloudification

Envelope spectrum analysis: Perform Hilbert envelope demodulation on each denoised signal segment $\widehat{x}_m[n](m = 1, \ldots, 10)$ according to Equations (6)–(9) and calculate the envelope spectrum $S_m(f)$. Taking data segment 3 as an example, its envelope spectrum shows obvious peaks at the fault frequency $f_{BPFI} \approx 250.5$ Hz and its double frequency $2f_{BPFI} \approx 501.0$ Hz. However, it is still disturbed by background noise spectral lines, as shown in **Figure 3**.

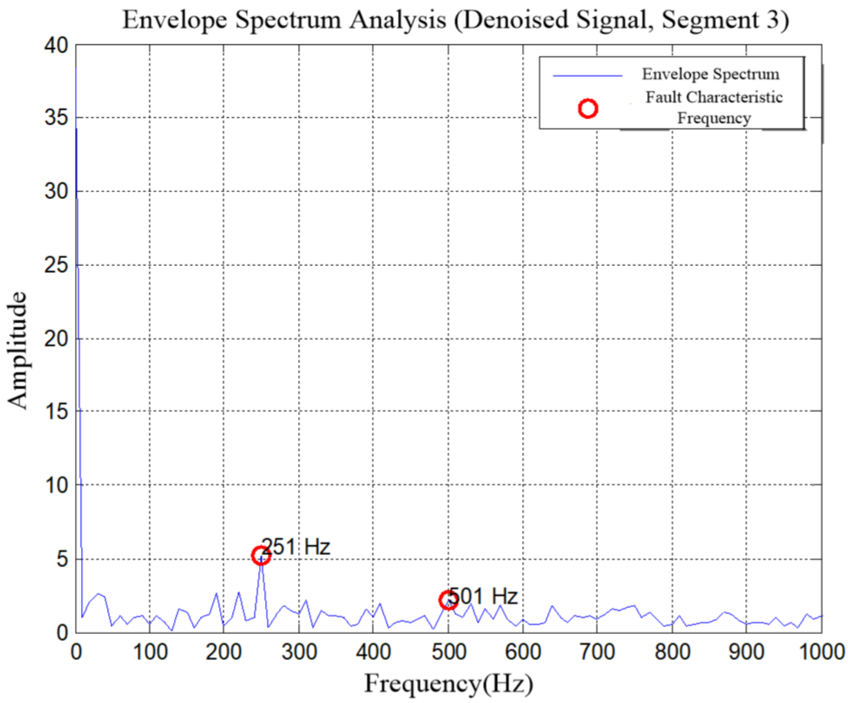

Figure 3. Hilbert envelope spectrum of the 3rd segment denoised signal.

Figure 3 shows the Hilbert envelope spectrum of the 3rd segment denoised signal. The abscissa is the frequency range of 0–1,000 Hz. The ordinate is the envelope spectrum amplitude. The blue curve is the overall distribution of the envelope spectrum. The red dots mark the fault characteristic frequency positions. Obvious peaks appear at 250.5 Hz, inner ring fault fundamental frequency, and 501.0 Hz, double frequency. The fundamental frequency peak is much higher than the background noise spectral line. The double frequency peak is also clearly distinguishable. There are no obvious clutter peaks in other frequency bands. This indicates that after Hilbert envelope demodulation, the denoised signal successfully extracts the characteristic frequency components matching the bearing inner ring fault. Even with a small amount of background noise interference, the fault frequency has high identifiability. This provides a reliable spectrum basis for the subsequent calculation of fault feature peak factors.

Calculate fault feature peak factor: Calculate the characteristic peak factor $F_{BPFI}^{(m)}$ of each data segment for inner ring faults according to Equation (10). Take $W = 2$, considering fundamental frequency and double frequency, $N_f = 1,280$. The calculation results are shown in **Table 3**.

Table 3. Peak factors of inner ring fault characteristics for each data segment.

Data segment	1	2	3	4	5	6	7	8	9	10
$F_{BPFI}^{(m)}$	7.117	8.143	9.264	10.221	9.894	8.015	10.994	10.790	9.437	9.923

For **Table 3**, set the threshold to 1.0 and the mean value to 9.380, expected value. The $F_{BPFI}^{(m)}$ values of each data segment are much higher than the fault identification threshold of 1.0. They are distributed between 7.117 and 10.994, showing small fluctuation characteristics as a whole. The 7th data segment reaches the peak value. The 1st data segment is the minimum value. The other segments fluctuate up and down around the expected value. This shows the stability and volatility of fault features. The overall high value of the peak factor verifies that fault features are effectively extracted in each signal segment. The small fluctuation reflects the inherent uncertainty of feature extraction in strong noise environments.

CM characterization: Take the 10 $F_{BPFI}^{(m)}$ values in **Table 3** as samples. Perform inverse cloud transformation according to Equations (11)–(13) to obtain the CM$C_{BPFI}\left(Ex_{BPFI}, En_{BPFI}, He_{BPFI}\right)$ characterizing the inner ring fault feature peak factor. $Ex_{BPFI} = (7.117 + 9.923 + \ldots)/10 = 9.380$, $En_{BPFI} = \sqrt{\pi/2} \times \left(|7.117 - 9.380| + \ldots + |9.923 - 9.380|\right)/10 \approx 1.248$; Sample variance $S^2 = \frac{1}{9}\sum\left(F^{(m)} - 9.380\right)^2 \approx 1.598$, $He_{BPFI} = \sqrt{S^2 - En_{BPFI}^2} = \sqrt{1.598 - 1.558} \approx 0.285$. Finally, $C_{BPFI}(9.380, 1.248, 0.285)$ is obtained.

This CM indicates that the expected value of the inner ring fault feature factor is 9.380. The entropy 1.248 indicates that its typical fluctuation range is approximately [8.13, 10.63]. The hyper-entropy 0.285 is small, indicating that the entropy estimation is relatively stable.

Step 3: Cloudified feature factor input to SFN

Construct SFN model: Establish a simplified fault evolution describing train axle box overheating alarm caused by early pitting of bearing inner rings. The network structure refers to the SFEP analysis method [21]. Edge events V_e: e_1 micro-damage occurs on the bearing inner ring, affected by feature factor C_{BPFI}; e_2 poor lubrication, environmental factor, set to constant probability $p_2 = 0.05$. Process events V_p: e_3 intensified bearing vibration; e_4 abnormal bearing temperature rise. Final event V_f: e_5 axle box overheating alarm, system-level fault. Logical relationships: $e_3 = e_1$OR e_2, intensified vibration can be caused by inner ring damage or poor lubrication; $e_4 = e_3$ AND $tp_{3\to4}$, abnormal temperature rise evolves from intensified vibration under specific conditions, set $tp_{3\to4} = 0.8$; $e_5 = e_4$ AND $tp_{4\to5}$, overheating alarm is triggered by abnormal temperature rise, set $tp_{4\to 5} = 0.9$.

Define cloudified feature function: For edge event e_1, its occurrence probability is affected by cloudified feature factor C_{BPFI}. Define the cloudified feature function according to Equation (14). Set threshold $\theta_{1,BPFI} = 1.0$, adjustment coefficient $\eta = 2.5$. We have $Ex_{1,EPFI}^{P} = \Psi\left(\frac{9.380-1.0}{2.5 \times 1.248}\right) = \Psi(2.685) \approx 0.996$.

Further, the entropy and hyper-entropy are $En_{1,BPFI}^{p} = 0.145$ and $He_{1,BPFI}^{P} = 0.048$ respectively. Obtain $P_{1,BPFI}^{\text{cloud}}(0.996, 0.145, 0.048)$. That is, the occurrence probability of inner ring damage event e_1 is about 99.6% with certain uncertainty.

Calculate the CM of edge event occurrence probability: $P^{\text{cloud}}(e_1) = P_{1,BPFI}^{cloud} = (0.996, 0.145, 0.048)$, $P^{\text{cloud}}(e_2) = 0.05$, definite value, can be regarded as a cloud with entropy and hyper-entropy of 0 (0.05, 0,0).

Probability propagation and final event probability calculation: $P^{\text{cloud}}(e_3)$: $e_3 = e_1$ OR e_2, simplify calculation by setting $tp_{1\to 3} = 1$, $tp_{2\to 3} = 1$. Perform cloud drop operation according to Equation (17). Generate $N_{\text{drop}} = 10,000$ cloud drops from $P^{\text{cloud}}(e_1)$ and $P^{\text{cloud}}(e_2)$ respectively. For $P^{\text{cloud}}(e_1)$, each cloud drop is generated by first generating a normal random number En' with $En_{1,BPFI}^{P}$ as the expectation and $He_{1,BPFI}^{P}$ as the standard deviation. Then generate a normal random number with $Ex_{1,BPFI}^{P}$ as the expectation and En' as the standard deviation as the value $p_1^{(i)}$ of the cloud drop. The cloud drops of $P^{\text{cloud}}(e_2)$ are all 0.05. For each pair of cloud drops $\left(p_1^{(i)}, p_2^{(i)}\right)$, calculate $p_3^{(i)} = 1 - \left(1 - p_1^{(i)}\right) \cdot \left(1 - p_2^{(i)}\right)$. Perform forward cloud transformation on the obtained 10,000 $p_3^{(i)}$, calculate their mean value, $\sqrt{\pi/2}$ times the first-order absolute central moment, variance, etc., to obtain the digital characteristics of $P^{\text{cloud}}(e_3)$. The calculation result is $P^{\text{cloud}}(e_3) \approx (0.944, 0.082, 0.032)$. Calculate $P^{\text{cloud}}(e_4)$: $e_4 = e_3$ AND $tp_{3\to 4}$. Perform cloud drop operation according to Equation (16). $tp_{3\to 4} = 0.8$ is a definite value. For each $p_3^{(i)}$, calculate $p_4^{(i)} = p_3^{(i)} \times 0.8$. Perform forward cloud transformation on the resulting cloud drop set. The calculation result is $P^{\text{cloud}}(e_4) \approx (0.755, 0.066, 0.025)$.

Figure 4 shows the comprehensive results of the CM. The upper part is the cloud drop distribution histogram of the fault feature peak factor. Cloud drops are concentrated between 8 and 11, showing normal distribution characteristics around the expected value 9.380. The narrow tails on both sides indicate that the dispersion degree of the feature factor is small. This is consistent with the quantitative results of entropy 1.248 and hyper-entropy 0.285, verifying the rationality of the CM. The lower part is the bar chart of the expected occurrence probability values of each event $(e_1 - e_5)$. The black error bars are entropy values. The expected probability value of e_1 is the highest (0.941). It decreases stepwise with fault evolution to e_5, except e_2. Finally, the expected probability value of e_5, axle box overheating alarm, is 0.680. The error bars of each event are narrow, indicating that the uncertainty of each event probability estimation is low. This figure converts abstract CM parameters into intuitive graphics, showing the uncertainty distribution of fault features and the probability transmission law in the SFEP.

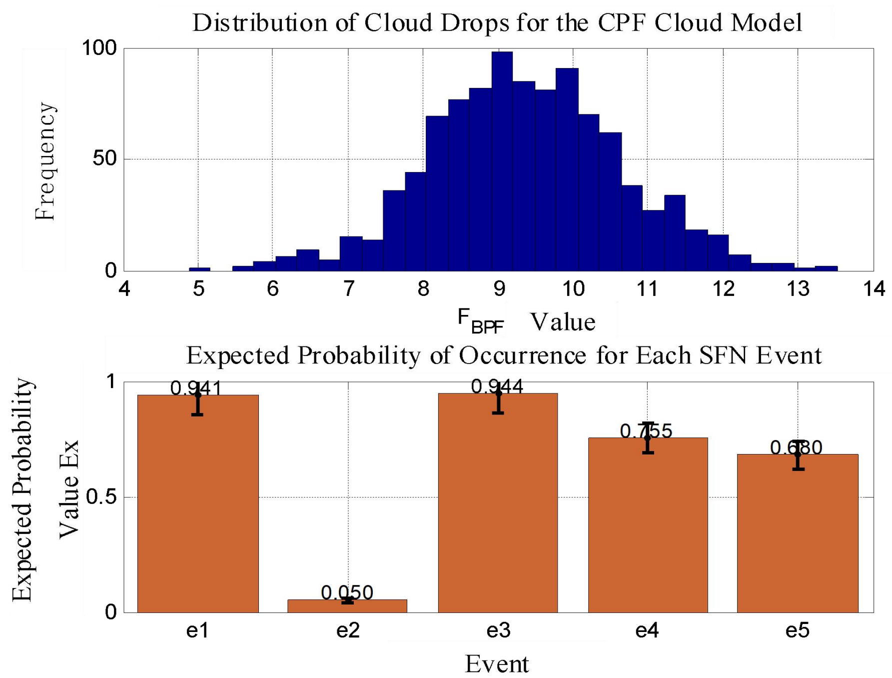

Figure 4. Fault feature CM and probability CM of each event.

Calculate the final event probability $P_T^{\text{cloud}} = P^{\text{cloud}}(e_5)$: $e_5 = e_4$ AND $tp_{4\to5}$, $tp_{4\to5} = 0.9$. For each $p_4^{(i)}$, calculate $p_5^{(i)} = p_4^{(i)} \times 0.9$. The final result is $P_T^{\text{cloud}} = (Ex_T, En_T, He_T) \approx (0.680, 0.059, 0.023)$.

4.3. Summary of case analysis

Effectiveness of feature extraction: Under strong noise of -5 dB, the fault feature peak factor F_{BPFI} of early bearing inner ring faults is extracted through FSE-based wavelet denoising and envelope spectrum analysis. The expected value $Ex = 9.380$ of its CM is significantly higher than the threshold 1.0. This indicates that fault features have been effectively detected.

Evolution risk quantification: Input the cloudified feature factor C_{BPFI} $(9.380, 1.248, 0.285)$ into the preset SFN evolution model. Obtain the CM of system fault, axle box overheating alarm, occurrence probability through cloud algebra operation as $P_T^{\text{cloud}}(0.680, 0.059, 0.023)$.

Decision support: 1) The expected value of the final fault probability $Ex_T = 0.680$. This indicates that under the current early fault features, the system has about 68.0% probability of evolving to an overheating alarm state with a high risk level. It is recommended to trigger an early warning and conduct inspection. 2) Uncertainty evaluation: The entropy $En_T = 0.059$ is small, indicating that the fluctuation range of this probability estimation is narrow and the conclusion is relatively definite. The hyper-entropy $He_T = 0.023$ is very small, indicating that the uncertainty evaluation itself is also very reliable.

To better evaluate the relative performance of the proposed method in terms of noise suppression and feature preservation, comparative experiments with classical wavelet soft-threshold denoising (WSTD) and ensemble empirical mode decomposition (EEMD) are supplemented. Under the same simulation conditions (SNR = -5 dB

Gaussian white noise), the performance comparison of different methods is shown in **Table 4**.

Table 4. Performance comparison of different methods under −5 dB noise.

Method	Mean F_{BPFI}	Std F_{BPFI}	Mean ΔSNR (dB)
Original Noisy Signal	5.700	0.841	—
WSTD	50.572	29.075	5.0
EEMD	4.334	0.891	−0.9
Proposed Method	9.380	1.265	5.0

The proposed method (FSE + CM + SFN) achieves a fault characteristic peak factor (F_{BPFI}) mean of 9.380, which is significantly higher than that of the original noisy signal (5.700) and the EEMD result (4.334). Moreover, its standard deviation (1.265) is much lower than that of the WSTD result (29.075), indicating more stable feature extraction. In terms of signal-to-noise ratio improvement, both the proposed method and WSTD achieve 5.0 dB, while EEMD fails to effectively suppress noise (ΔSNR = −0.9 dB). The results demonstrate that the proposed method achieves the best balance between noise suppression and fault feature preservation under strong noise, with overall performance superior to traditional methods.

It is noteworthy that the mean F_{BPFI} of the WSTD method (50.572) in **Table 1** is abnormally high, but its standard deviation (29.075) is extremely large. This indicates that the classical wavelet soft-thresholding, when processing the −5 dB strong noise signal in this study, may suffer from over-filtering due to its fixed global threshold. This not only suppresses noise but may also unreasonably amplify certain residual signal components or severely distort the morphology of the envelope spectrum, resulting in distorted and unstable high feature values. This phenomenon reveals the limitations of traditional thresholding methods in extreme noise environments, where parameter adaptation is difficult, leading to overfitting or the introduction of false characteristics. In contrast, the adaptive threshold strategy based on the fuzzy structured element in the proposed method achieves a better balance between noise suppression and retention of genuine fault impacts. Therefore, although its feature value (9.380) is lower than that of WSTD, it is more authentic and stable, and its standard deviation (1.265) falls within a reasonable range, reflecting the repeatability and reliability of the feature extraction process.

4.4. Parameter sensitivity analysis and selection strategy

To ensure the reproducibility of the proposed method and its applicability to different systems, this section discusses and analyzes the selection of key parameters. The main parameters involved include: the wavelet basis function, decomposition level, threshold adjustment factors in the wavelet denoising module; and the number of cloud drops in cloud algebra operations.

(1) Wavelet denoising parameters: The choice of wavelet basis function affects the matching degree to local signal features. For bearing fault impulse signals, the Daubechies (dbN) family wavelets are often adopted due to their compact support and approximate symmetry. Based on preliminary experiments comparing db5,

db8, and db10 under the same decomposition level in terms of reconstruction error and feature preservation for the simulated signal, db10 was found to achieve a slightly better balance in this case. The decomposition level determines the granularity of detail extraction. Too many levels may cause over-decomposition and introduce spurious components, while too few may insufficiently separate noise. Referring to the empirical formula (level $\leq \log 2(N)$, where N is the number of signal points) and combined with trial-and-error, the decomposition level of 5 was selected, which can effectively capture the frequency band containing fault impulses for the 2,560-point signal length. The threshold adjustment factors control the shape of the improved threshold function (Equation (15)) between soft and hard thresholds. Their values affect the aggressiveness of denoising: larger factor values make the function closer to the hard threshold, potentially preserving more details but also possibly introducing artifacts; smaller values lead to smoother results. Through grid search, using both the SNR improvement of the denoised signal and the stability of the characteristic peak factor as dual indicators, it was determined that under the current −5 dB noise environment, values of the threshold adjustment factors within the interval $[1, 2]$ yield robust performance. The program uses a value of 1. The grid search method here draws on the approach of determining optimal values through parameter sensitivity analysis in related research (e.g., the analysis of parameters c_3 and c_4 [25,26]).

(2) Cloud Algebra operation parameter: The number of cloud drops affects the statistical stability of cloud model operations (forward cloud transformation and cloudified characteristic function calculation). Too small a number leads to large fluctuations in probability distribution estimation; too large increases unnecessary computational overhead. Referencing common practices in cloud model applications [19] and testing the variation of the expected value and entropy of the final fault probability cloud model with the number of cloud drops ranging from 1,000 to 20,000, it was found that when the number of cloud drops is no less than 5,000, the expected value and entropy stabilize with a standard deviation less than 0.005. To ensure sufficient accuracy, a number of 10,000 cloud drops is used in this paper. Parameter sensitivity analysis is crucial for ensuring model performance, and similar analytical methods are widely used in other fault diagnosis models.

In summary, the parameter selection in this paper is based on preliminary analysis of the current case signal characteristics. For different application scenarios (e.g., different noise levels, fault types), users are advised to conduct similar pre-analysis or grid search following the above principles to determine suitable parameters. Future work will focus on developing adaptive parameter selection rules based on signal characteristics (e.g., kurtosis, entropy).

5. Discussion

The advantage of the algorithm is that the constructed integrated framework of signal denoising-feature cloudification-evolution evaluation realizes weak fault feature extraction and SFEP evaluation under strong noise. It has a logical closed loop and meets the fault diagnosis requirements of complex industrial systems. The wavelet threshold denoising algorithm based on the FSE can adaptively distinguish noise and fault impact components. It realizes noise suppression and fault feature retention. The characterization of fault feature factors by the CM encapsulates the randomness and fuzziness of the feature extraction process. It realizes uncertainty quantification. The integrated operation of SFN and cloud algebra completes the effective transmission of fault feature uncertainty in the SFEP. It realizes fault probability evaluation.

The shortcomings of the algorithm are that the data do not consider non-Gaussian noise and multi-fault coupling in actual scenarios. The wavelet basis function and decomposition layer number are manually set, which easily affects the denoising effect.

Furthermore, the proposed method in this paper has currently been validated only on simulated bearing inner ring fault data with additive Gaussian white noise. Its generalization capability to other common fault types (e.g., outer ring fault, rolling element fault) and to other more complex noise types prevalent in practical scenarios (e.g., non-Gaussian noise, colored noise, impulsive noise) has not been systematically examined. Future work will focus on:

(1) Applying this framework to a broader range of fault simulation scenarios, including simulations of bearing outer ring and rolling element faults based on dynamic models [27], as well as gear fault simulations [28];
(2) Investigating the robustness of the method under various noise environments and considering adaptations of the Fuzzy Structured Element-based wavelet threshold denoising model to handle non-stationary and non-Gaussian noises.

The event logic and transmission probability are empirically set without combining the actual system fault statistics. The number of cloud drop operations is a fixed value. The background amplitude estimation of envelope spectrum analysis adopts fixed coefficient correction, which has poor adaptability to different fault types. The solutions to the above shortcomings are: introduce non-Gaussian noise and add multi-fault impact signals to improve data authenticity; establish a multi-index evaluation system for wavelet parameters to realize adaptive matching of basis functions and decomposition layers; optimize SFN transmission probability using Bayesian method combined with industrial data; dynamically adjust the number of cloud droplets in the cloud algebra calculation based on the entropy of the CM according to the CM entropy value; establish background amplitude correction coefficients for different fault types to realize adaptive amplitude estimation.

In addition, the case data in this paper are all generated by laboratory calibration. The case SFN only contains 5 event nodes. Laboratory calibration data can accurately control variables such as noise and fault types, eliminate complex interference, and focus on verifying the effectiveness of the core logic of the method. Simplified SFN can reduce model complexity, clearly present the core causal relationship of fault evolution, and avoid redundant nodes covering key logic. This idea of control variables-simplified model can ensure the validity of the core algorithms and framework. Subsequent research can introduce measured data and complex network structures.

Theoretically, this study deeply integrates the FSE, CM and SFN. It improves the extraction and quantification methods of uncertain fault features under strong noise. It provides a mathematical model and analysis idea for fault evolution analysis. The integrated analysis framework realizes the connection between signal processing and fault evolution evaluation. It provides a method for uncertainty analysis of fault diagnosis. In engineering, the method can effectively extract early weak fault features of bearings under strong noise. It can provide technical support for early fault warning of complex systems such as high-speed trains and aero-engines. The fault probability CM can provide multi-dimensional risk information including central estimation and uncertainty. It provides a quantitative basis for maintenance and safety decision-making.

This case study aims to validate the proposed integrated Fuzzy Structured Element-Cloud Model-Spatial Fault Network framework's capability for extracting weak fault features, quantifying uncertainty, and assessing system evolution under strong noise (SNR $= -5$ dB). To achieve this, it is necessary to generate time-series data containing a clear fault characteristic frequency, with a known high-intensity noise level and a regular signal structure. Most public bearing fault datasets (e.g., the widely used CWRU dataset and Paderborn University (PU) dataset) primarily provide raw vibration waveforms collected under relatively favorable laboratory conditions, with typically lower background noise (higher SNR). Their data structures significantly differ from the input requirements of this study's focus on the strong noise-weak impulse-evolution assessment chain. The main differences are:

(1) Different noise environment: Public datasets are usually acquired in controlled settings with low background noise, whereas this study focuses on validating method performance under extreme strong noise (SNR $= -5$ dB);
(2) Different data dimensions and objectives: Public datasets often consist of long time-series raw vibration acceleration or acoustic signals from single sensors, primarily used for fault classification or detection [29], where noise is added to CWRU data and sliding window processing is applied for classification]. In contrast, our framework requires input signals segmented (10 segments in this case), each containing specific fault impulse patterns, and outputs cloudified features and network evolution probabilities, emphasizing the assessment of the uncertainty evolution process rather than mere health state classification;
(3) Controllability of feature weakness: The fault impulse amplitude in public datasets is usually fixed, making it difficult to adjust on demand to simulate weak features. Therefore, directly using these datasets hinders precise control over noise level and fault impulse weakness to validate the core links of our framework.

Consequently, this study employs dynamic simulation based on fault mechanisms to generate data. When constructing the simulation model, the bearing's geometric parameters, operating speed, and the calculation of the fault characteristic frequency strictly adhere to industry standards and common parameter settings from public datasets (CWRU dataset and Paderborn University (PU) dataset), referencing the idea of generating fault data through parametric models in digital twin modeling [30].

Meanwhile, to simulate the strong noise environment and construct data meeting the framework's input requirements, the following data supplementation and reconstruction operations were performed:

(1) Active noise injection: Gaussian white noise with an SNR of −5 dB is actively added to the generated simulation signal, consistent with the practice of adding noise to public datasets to test model robustness in many studies [29];
(2) Signal segmentation and reconstruction: The total 2 s simulated signal is equally divided into 10 consecutive 0.1 s data segments (corresponding to 10 data segment signals) to mimic the continuous observation and analysis process in practical engineering. This segmentation approach is similar to the method of dividing long time-series data using sliding windows to construct samples [31];
(3) Feature frequency calibration: The final calibrated simulation model ensures the accuracy of the generated fault impulse's corresponding characteristic frequency, which aligns with the principle of confirming fault frequencies when using public datasets. This controlled data generation strategy, which references public dataset standards and incorporates targeted supplementation and reconstruction, ensures targeted validation of the logical correctness and effectiveness of the methodological chain presented in this paper under the defined harsh scenario.

The proposed method in this study has currently been validated on simulated bearing inner ring fault data with additive Gaussian white noise. Although the simulation data generation strictly referenced parameter standards from public datasets and actively injected high-intensity noise to construct the target scenario [27], there are differences between the simulation environment (particularly Gaussian white noise) and the more complex noise characteristics (e.g., non-Gaussian, colored, or impulsive noise) encountered in practical engineering. Furthermore, the generalization capability of the method to other fault types (e.g., outer ring, rolling element faults) requires further examination. These constitute the current limitations of this work.

To enhance the credibility and generalizability of the method, future research will focus on:

(1) Testing the framework under a wider range of fault simulation scenarios, including bearing outer ring and rolling element fault simulations based on dynamic models [27] as well as gear fault simulations [28];
(2) Applying the method to public bearing fault benchmark datasets (e.g., the Case Western Reserve University CWRU dataset [29]) or self-collected test-rig data to verify its performance on real or quasi-real vibration signals;
(3) Investigating the adaptability of the method to non-stationary, non-Gaussian noise environments, and further refining the fuzzy structured element-based wavelet threshold denoising module.

6. Conclusion

(1) A three-in-one weak fault analysis framework and mathematical model under strong noise are constructed. It integrates the theories of FSE, CM and SFN.

A FSE wavelet threshold denoising model is established to realize fault signal recovery under strong noise. A cloudification characterization method for fault feature peak factors is designed to complete the quantification of feature extraction uncertainty. A cloudified feature function and SFN probability propagation model are constructed to realize the quantitative transmission of uncertainty in the SFEP. This provides theoretical and algorithm support for fault diagnosis of complex systems.

(2) Taking the inner ring pitting fault vibration of axle box bearings as an example, the effectiveness and engineering applicability of the method are verified. Under strong noise of SNR = -5 dB, the 250.5 Hz fault characteristic frequency and double frequency components are successfully extracted. The feature peak factor CM (9.380,1.248,0.285) can stably characterize fault features. The system fault probability CM (0.680,0.059,0.023) is obtained through SFN probability propagation, quantifying the fault evolution risk and evaluation reliability. Compared with the traditional WSTD and EEMD methods, the proposed method achieves more stable feature extraction and better noise reduction effect, which confirms its superiority in strong noise environments.

(3) The method has significant theoretical and engineering application value. Theoretically, it realizes the deep integration of FSE, CM and SFN. It improves the extraction and evolution analysis of uncertain fault features under strong noise. In engineering, it solves problems such as weak fault feature extraction and evolution uncertainty quantification. It is suitable for fault diagnosis and risk assessment of complex industrial systems. It provides a technical path for equipment maintenance and safety decision-making.

(4) The parameter sensitivity analysis clarifies the selection criteria of key parameters such as wavelet basis function, decomposition layer and cloud drop number, which ensures the reproducibility of the model. The applicability analysis of public datasets explains the difference between simulation data and actual data, and provides a standardized data processing scheme for engineering application, which lays a foundation for the further extension of the method to multi-fault and non-Gaussian noise scenarios.

Author contributions: Conceptualization, TC and SL; methodology, TC; software, ZC; validation, TC; formal analysis, SL; investigation, ZC; resources, SL; data curation, ZC; writing—original draft preparation, TC; writing—review and editing, SL; visualization, TC; supervision, SL; project administration, SL; funding acquisition, SL. All authors have read and agreed to the published version of the manuscript.

Funding: This study was partially supported by Liaoning Provincial Science and Technology Plan Joint Program (Natural Science Foundation-General Program 2025-MSLH-584) and Funded by the Fundamental Research Funds for Liaoning Provincial Undergraduate Universities (Grant Nos. LJ212410144051; LJ212410144032).

Institutional review board statement: Not applicable.

Informed consent statement: Not applicable.

Data availability statement: The data is unavailable due to privacy or ethical restrictions.

Conflict of interest: The authors declare no conflict of interest.

AI use statement: The authors declare that no artificial intelligence (AI) tools were used in the preparation of this manuscript.

References

1. Zou M, Zhou B, Dai M, et al. An adaptive signal processing framework for fault diagnosis: Intelligent spectral optimization for robust weak periodic feature extraction from vibration signals. Digital Signal Processing. 2026; 176: 106055. doi: 10.1016/j.dsp.2026.106055
2. Zhang K, Li M, Jin F, et al. Variational filtering differential strategy with amplitude modulation for fault feature extraction. Measurement Science and Technology. 2026; 37(10): 106105. doi: 10.1088/1361-6501/ae4cbb
3. Wang Z, Yu X, Guo Y, et al. Research on a novel weak fault detection method based on vibrational resonance in high-dimensional chaotic system, and variational mode decomposition. Chaos, Solitons & Fractals. 2026; 208: 118084. doi: 10.1016/j.chaos.2026.118084
4. Liu L, Xu H, Guo P, et al. GE-HOFMD fusion-based early fault feature extraction and diagnosis for rolling bearings. Engineering Research Express. 2026; 8(4): 045513. doi: 10.1088/2631-8695/ae42ec
5. Shi G, Qin C, Xia P, et al. Generalized envelope nonlinear Gini index-gram guided two-stage chirp mode decomposition for shield machine main bearing fault diagnosis. Advanced Engineering Informatics. 2026; 71: 104354. doi: 10.1016/j.aei.2026.104354
6. Liu Y, Zhou Y, Hu T, et al. A weak-fault diagnosis method for bearings based on quadratic Manhattan entropy. Measurement. 2026; 264: 120242. doi: 10.1016/j.measurement.2025.120242
7. Guo D, Chen J, Liu X, et al. Research on Rolling Bearing Fault Diagnosis Based on IRBMO-CYCBD. Mathematics. 2026; 14(1): 201. doi: 10.3390/math14010201
8. Zou Y, Zhang Y, Li CF, et al. A multi-scale dilated convolutional neural network-based bearing fault diagnosis method with dense connections under strong noise conditions. Measurement Science and Technology. 2026; 37(7): 076110. doi: 10.1088/1361-6501/ae44bd
9. Chen Y, Zhang W, Cao Z, et al. Multi-scale adaptive quadratic convolutional network: reliable gearbox fault identification under severe noise. Measurement Science and Technology. 2026; 37(6): 066101. doi: 10.1088/1361-6501/ae412d
10. Wang H, Fang G, Cui X, et al. Parallel Axial Attention and ResNet-Based Bearing Fault Diagnosis Method. Electronics. 2026; 15(4): 899. doi: 10.3390/electronics15040899
11. Xu Z, Chen Z, Li X, et al. EPA-RepViT: A lightweight model for fault diagnosis of planetary gearbox under strong noise. Engineering Research Express. 2026; 8(1): 015207. doi: 10.1088/2631-8695/ae29bd
12. Li Z, Li P, Yang J, et al. Auditory perception–based acoustic fault diagnosis for railway wheelset bearings under strong noise: a comparison with short-time Fourier transform, Mel spectrogram, and continuous wavelet transform. Engineering Research Express. 2026; 8(2): 025508. doi: 10.1088/2631-8695/ae35d7
13. Dong H, Zhang Y, Zhang B, et al. A noise-robust xLSTM-based method for fault diagnosis in gas-insulated Switchgear using acoustic signals under strong noise interference. Expert Systems with Applications. 2026; 304: 130827. doi: 10.1016/j.eswa.2025.130827
14. Li M, Huang J, Zhang F, et al. MSIF-Convformer: A novel end-to-end fault diagnosis framework with multi-source sensors under strong noise. Information Fusion. 2026; 129: 104000. doi: 10.1016/j.inffus.2025.104000
15. Zhao L, Liu Y, Zhang Z, et al. Nonlinear convolutional sparse filtering with Gaussian fitting for rolling bearings compound fault diagnosis. Structural Health Monitoring. 2026; 25(1): 516–536. doi: 10.1177/14759217241286087
16. Li S, Wang T, Xu X, et al. An Improved DQN Framework with Dual Residual Horizontal Feature Pyramid for Autonomous Fault Diagnosis in Strong-Noise Scenarios. Sensors. 2025; 25(24): 7639. doi: 10.3390/s25247639
17. Cui T, Wei P, Li S. Partial differential analytical expression for the failure rate change of electrical components under multi-fault coupling. Advances in Differential Equations and Control Processes. 2025; 32(3). doi: 10.59400/adecp3444

18. Guo S, Song T. Operations and Measurement of Interval-valued Fuzzy Numbers Based on the Method of Structured Element. Fuzzy Information and Engineering. 2011; 3(1): 101–110. doi: 10.1007/s12543-011-0069-6
19. Li D, Liu C, Gan W. A new cognitive model: Cloud model. International Journal of Intelligent Systems. 2009; 24(3): 357–375. doi: 10.1002/int.20340
20. Si Y, Zhang Z, Kong L, et al. Aging condition identification of viscoelastic sandwich structure based on empirical wavelet transform and Hilbert envelope demodulation. Composite Structures. 2019; 215: 13–22. doi: 10.1016/j.compstruct.2019.02.039
21. Cui TJ, Li S. Deep learning of system reliability under multi-factor influence based on space fault tree. Neural Computing and Applications. 2019; 31(9): 4761–4776. doi: 10.1007/s00521-018-3416-2
22. Jang J, Lee H. Resilient fault diagnosis and recovery framework for driving modules of electric vehicles using continuous wavelet transform-based fault-aware deep learning. Applied Soft Computing. 2026; 198: 115289. doi: 10.1016/j.asoc.2026.115289
23. Fang C, Liang Y, Zhou W, et al. Dynamic and contact characteristics of axle-box bearing for a high-speed train under wheel polygonization. Mechanism and Machine Theory. 2026; 224: 106437. doi: 10.1016/j.mechmachtheory.2026.106437
24. Cui TJ, Li SS. Study on the construction and application of discrete space fault tree modified by fuzzy structured element. Cluster Computing. 2019; 22(S3): 6563–6577. doi: 10.1007/s10586-018-2342-5
25. Mallat SG. A theory for multiresolution signal decomposition: the wavelet representation. IEEE Transactions on Pattern Analysis and Machine Intelligence. 1989; 11(7): 674–693. doi: 10.1109/34.192463
26. Zheng FL, Pan HY, Zheng JD, et al. Fuzzy projection twin broad learning and its application to rolling bearing fault diagnosis. 2025; 44(08): 192–198. doi: 10.13465/j.cnki.jvs.2025.08.021 (in Chinese)
27. Chen J, Cao Z, Liu YB, et al. Multi-degree-of-freedom dynamic modeling of ball bearing with rolling element spalling defect. Journal of Machine Design. 2026; 43(01): 53–61. doi: 10.13841/j.cnki.jxsj.2026.01.009 (in Chinese)
28. Huang K, Li A, Zhu G, et al. A comprehensive review of fractal theory in gear transmission: From microscopic contact to fault diagnosis. Engineering Research Express. 2025; 7(4): 042505. doi: 10.1088/2631-8695/ae2239
29. Zhao GC, Liu CD, Song YN, et al. Bearing fault diagnosis method based on fusion of time-frequency features by cross-attention mechanism. Journal of Vibration and Shock. 2025; 44 (12): 228–237. doi: 10.13465/j.cnki.jvs.2025.12.024 (in Chinese)
30. Liu SY, Dong YL, Qiao YM, et al. Research on Dynamic Fault Injection of Bearing Digital Twin Model Based on Improved Dung Beetle Optimization Algorithm. Journal of Mechanical Engineering. 2026; 62(03): 446–457. Available online: http://www.cjmenet.com.cn/CN/10.3901/JME.260097 (in Chinese)
31. Lei Y, Yang B, Jiang X, et al. Applications of machine learning to machine fault diagnosis: A review and roadmap. Mechanical Systems and Signal Processing. 2020; 138: 106587. doi: 10.1016/j.ymssp.2019.106587